IEEE Transactions on Industry Applications,
Volume 58, Number 3, May-June 2022, pp. 3674-3684
DOI: 10.1109/TIA.2022.3160680

Servo Control of Drive-Trains Incorporating Magnetic Couplings

Xiaowen Liao
Guangdong University of Petrochemical Technology (GDUPT) and Joint Research Lab between GDUPT and University of Lincoln
Maoming, China
email: xliao@lincoln.ac.uk

Chris Bingham
School of Engineering
University of Lincoln
Lincoln, UK
email: cbingham@lincoln.ac.uk

Argyrios Zolotas
Systems and Control Centre
Cranfield University
Cranfield, UK
email: A.Zolotas@cranfield.ac.uk

Qinghua Zhang
School of Automation
Guangdong University of Petrochemical Technology
Maoming, China
email: fengliangren@tom.com

Tim Smith
School of Engineering
University of Lincoln
Lincoln, UK
email: tismith@lincoln.ac.uk

***Abstract*—The paper presents a high performance and low-cost design methodology for the servo control of magnetic drive-trains (MDTs) operating in direct drive mode. For the first time, this paper considers using sensitivity peaks to analyse the robustness and stability of MDT control systems. Initially, through analysis of a dynamic model, the key spring characteristic parameters with respect to operating points, are developed. It is also shown that a wider dynamic performance envelope can be achieved by linearizing the MDT model at around 60%-80% of the maximum coupling torque, as opposed to traditional linearization under zero torque conditions. Subsequently, the paper exploits the spring characteristics for a design methodology based on the H_∞ mixed sensitivity approach to determine suitable control parameters. Following this, the maximum exogenous load-torque disturbance and speed reference that will not induce pole-slipping can be determined. Finally, preferential position reference profiles and optimal gains for position controllers are given to prevent demand-induced speed oscillations. The proposed methodologies are validated through simulation and experimental studies.**

***Index Terms*—Magnetic coupling, linearization, spring dynamics, two-degree-of-freedom PI, H_∞ mixed sensitivity, servo control.**

I. Introduction

Drive-trains incorporating magnetic torque transfer components overcome inherent problems of traditional mechanical counterparts due to their ability to pole-slip rather than breaking or jamming as a result of over-torque conditions. To date, magnetic gears with low transmission ratios have been successfully deployed in hybrid electric vehicles [1], aerospace [2], and renewable energy [3], [4] applications. However, servo applications of drive-trains incorporating magnetic couplings, with an effective gear-ratio of 1:1, are seldom reported.

Magnetic drive-trains (MDTs) are traditionally modelled as two-mass systems [5] by linearizing under zero load-torque conditions. However, the torsional stiffness of the resulting two-mass system is then considered to be a constant, unlike the practical stiffness characteristics of MDTs which vary with developed load and actuation torque. To address issues caused by the nonlinear stiffness, [6] proposes a nonlinear control strategy based on a feedback linearizing control law. However, the resulting implementation requires sensing of shaft position on both sides of the MDT which is prohibitive practically due to cost, integration and isolation issues–ideally control schemes incorporating only primary (driving) side measurements (not load-side) are preferable.

Pseudo Derivative Feedback (PDF) controllers are known to improve the stiffness of two-mass systems, reduce the sensitivity of control effort to load disturbances and suppress overshoot for step command inputs [7]–[10], and have previously been reported for speed control of MDTs [5], [11]. However, [5], [11] overlook the sensitivity peaks from speed references and load-torque disturbances to control effort; hence, [12] finds that using a PDF control configuration, an MDT subject to low load-torque can enter a pole-slipping regime when a small incremental speed reference is commanded. A proposed remedial method, also given in [12], requires prior knowledge of real-time load-torque, which again is practically prohibitive.

[13]–[15] employ an observer-based speed controller for pseudo direct drives (PDDs), which is a variant of MDTs. To operate effectively, observer bandwidths should be set much greater than the resonant frequency of controlled system [16]; however, low-cost drivers cannot offer high performance computational units and high resolution position sensors. Moreover, controller parameters in [13]–[15] are optimized on the basis of the integral of time multiplied by absolute error (ITAE) performance index which aims to provide optimum step responses for speed tracking. This is applicable since PDDs can be regarded as reduction gears. Additionally, non-reversible mechanic gearboxes were adopted in these applications. Hence, load-torque disturbance handling can be neglected in the design. However, due to not directly incorporating an analysis of load-torque disturbance rejection

characteristics, the resulting controllers can lead to MDTs with a gear-ratio of 1:1 entering pole-slipping even when the applied load is far lower than the maximum specified coupling torque.

Using classical methods, designs to accommodate both disturbance rejection and reference tracking performance of a speed regulation system can be realized using a two-degree-of-freedom proportional-integral (2DOF PI) controller [17]–[20]. The low-pass pre-filter of a 2DOF PI controller performs input shaping which can prevent significant excitation of resonant dynamics. If load-side oscillations can be suppressed, the load-side speed of the MDT is approximately equal to that of the motor-side (load-side sensors are therefore no longer required), and a low-cost implementation is realizable. However, using input-shaping techniques to design an appropriate pre-filter requires the full exploitation of the dynamic properties of the system to accommodate of the nonlinear stiffness characteristics of the MDT.

[21] proposes a single-loop PDF position controller rather than a two-loop structure (nested speed and position control loops) that is widely adopted in servo applications. In [21] load-torque disturbances are estimated through use of a 'low bandwidth' observer. The estimated value is then fed-forward to eliminate position errors resulting from the disturbances. However, the accuracy of model parameters can significantly affect the precision of the resulting estimation, and hence performance.

The primary aim of this paper is therefore to provide a low-cost systematic speed and position control strategy for drive-trains incorporating magnetic couplings (a direct drive scenario without non-reversible gearboxes, which is considered a worst case for magnetic gear variants). The control algorithms are developed theoretically and verified on an experimental test-bed. The benefits of the presented approach are:

1) Through appropriate selection of operating points, a wide range of load characteristics can be accommodated without the need for load-side sensing.
2) The optimized selection of pre-filter and feed-forward dynamics of a 2DOF controller are determined with the spring characteristic parameters of the MDTs, which successfully suppresses the motor- and load-side speed oscillations and reduces the possibility of pole-slipping induced by aggressive reference command inputs.
3) The proposed PI parameter optimization, robustness and stability analysis methods allow controllers to be designed to satisfy specific performance specifications. In particular, high-torque actuation demands induced by controllers, both from references and load-torque disturbances, are investigated to avoid initiating pole-slipping.

II. Dynamic Model and Linearisation

A. Experimental rig

An MDT test facility has been commissioned (as shown in Fig.1) for controller/dynamics validation purposes, and this provides a focus for the underlying principles that are to be discussed. The magnetic coupling embedded in the rig has 5 pole-pairs (p), and the maximum (pull-out) coupling torque (T_G) is 1.6 N·m. The MDT rig will enter a pole-slipping regime when a combination of the driving torque (T_{em}) and load-torque (T_L) exceeds T_G. The experimental facility has load- and motor-side inertias (J_L and J_M) of 0.001 kg·m^2 and the load- and motor-side friction coefficients (B_L and B_M) are 0.003N·m/(rad/s). A 12-bit position measurement sensor is incorporated on the primary-side of the MDT and a 2nd actively controlled motor provides a variable load-torque. Table. I and Table. II show the key parameters of experimental rig. The algorithm proposed in this paper is downloaded to the primary-side drive to verify its performance. Hence, the algorithm is required to be developed with real-time performance.

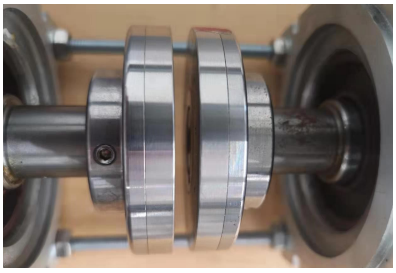

(a)

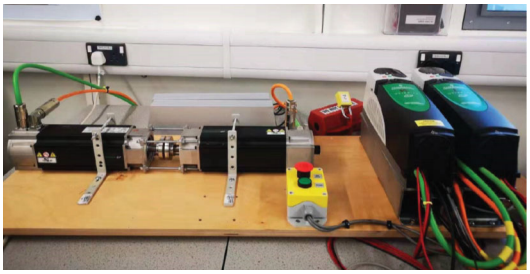

(b)

Fig. 1: Experimental test facility (a) magnetic coupling (b) motor and load side actuation.

TABLE I: Nameplate data of the converter under normal duty

Maximum continuous output current	Nominal power at 400V	Peak current
5.0 A	2.2 kW	5.5A

TABLE II: Nameplate data of the servo motor

Speed	Rated torque	Rated power	Torque constant	Poles
3000 rpm	6.8 N·m	2.14 kW	1.6 N·m/A	6

B. Model and linearisation

Primary-side speed and position are designated ω_M and θ_M, respectively, whilst load-side speed and position are designated ω_L and θ_L, respectively. Note: it is assumed that θ_L and ω_L are not measured for control purposes, as is desirable for most

MDT systems. Defining T_C as the torsional torque developed between the two sides of the MDT, then from [5]:

$$T_C = T_G \sin\left(p(\theta_M - \theta_L)\right) \tag{1}$$

If the damping torque T_D is significant, the MDT is described by the following set of equations (also from [5]):

$$\begin{aligned} \dot{\theta}_M &= \omega_M \\ \dot{\omega}_M &= \frac{1}{J_M}\left(T_{em} - T_C - B_M\omega_M - T_D\right) \\ \dot{\theta}_L &= \omega_L \\ \dot{\omega}_L &= \frac{1}{J_L}\left(T_C - T_L - B_L\omega_L + T_D\right) \end{aligned} \tag{2}$$

where $T_D = \alpha T_G \frac{2\beta(\omega_M - \omega_L)}{(\omega_M - \omega_L)^2 + \beta^2}$ (α is a proportion of maximum coupling torque capability, and β is the relative angular velocity at which maximum damping torque occurs).

Defining $x_1 = \theta_M$, $x_2 = \omega_M$, $x_3 = \theta_L$, $x_4 = \omega_L$, $u_1 = T_{em}$, $u_2 = T_L$, and $x = (x_1, x_2, x_3, x_4)^T$, $u = (u_1, u_2)^T = (T_{em}, T_L)^T$, (2) can be rewritten as

$$\dot{x} = f(x) + g(u) \tag{3}$$

where $f(x) = \begin{pmatrix} x_2 \\ \frac{1}{J_M}\left(-T_C - B_M x_2 - \alpha T_G \frac{2\beta(x_2 - x_4)}{(x_2 - x_4)^2 + \beta^2}\right) \\ x_4 \\ \frac{1}{J_L}\left(T_C - B_L x_4 + \alpha T_G \frac{2\beta(x_2 - x_4)}{(x_2 - x_4)^2 + \beta^2}\right) \end{pmatrix}$, and $g(u) = \begin{pmatrix} 0 \\ \frac{1}{J_M}u_1 \\ 0 \\ -\frac{1}{J_L}u_2 \end{pmatrix}$. If the damping torque is considered to be negligible ($\alpha = 0$) the state equations of (3) can be linearized to give:

$$\dot{x} = A_{lin}x + g(u) \tag{4}$$

where $A_{lin} = \begin{bmatrix} 0 & 1 & 0 & 0 \\ \frac{-K_{\text{lin}}}{J_M} & \frac{-B_M}{J_M} & \frac{K_{\text{lin}}}{J_M} & 0 \\ 0 & 0 & 0 & 1 \\ \frac{K_{\text{lin}}}{J_L} & 0 & \frac{-K_{\text{lin}}}{J_L} & \frac{-B_L}{J_L} \end{bmatrix}$, and K_{lin} is given by

$$K_{\text{lin}} = T_G p \cos(p(x_1 - x_3)) \tag{5}$$

Then, the resulting transfer function from T_{em} to ω_M is

$$G_{T_{em}}^{\omega_M}(s) = \frac{J_L s^2 + B_L s + K_{\text{lin}}}{A(s)} \tag{6}$$

where $A(s) = J_M J_L s^3 + (J_M B_L + B_M J_L)\, s^2 + (B_L B_M + (J_L + J_M)K_{\text{lin}})\, s + (B_M + B_L)K_{\text{lin}}$, and the transfer function from T_L to ω_M is given by

$$G_{T_L}^{\omega_M}(s) = -\frac{K_{\text{lin}}}{A(s)} \tag{7}$$

Assuming $B_L s$, $(B_M + B_L)K_{lin}$ and $B_M B_L$ are negligible, then (6) and (7) simplify to:

$$G_{T_{em}}^{\omega_M}(s) = \frac{1}{(J_M + J_L)\, s} \frac{(J_L + J_M)\, s^2 + J_M \omega_n^2}{J_M\left(s^2 + 2\zeta\omega_n s + \omega_n^2\right)} \tag{8}$$

$$G_{T_L}^{\omega_M}(s) = \frac{-1}{(J_M + J_L)\, s} \frac{\omega_n^2}{\left(s^2 + 2\zeta\omega_n s + \omega_n^2\right)} \tag{9}$$

where $\omega_n = \sqrt{\frac{K_{\text{lin}}(J_M + J_L)}{J_M J_L}}$, $\zeta = \frac{J_M B_L + B_M J_L}{2 J_M J_L \omega_n}$. Clearly, ω_n and ζ represent the natural frequency and damping ratio. Taking (8) and (9) into consideration and modeling $T_{em}(s)$ and $T_L(s)$ as step input signals ($T_{em}(s) = T_{em}/s, T_L(s) = T_L/s$), the motor-side speed response (in time domain) is given by

$$\omega_M(t) \approx \frac{T_{em} - T_L}{J_M + J_L} t + \frac{T_L + T_{em} J_L / J_M}{\omega_d} e^{-\zeta\omega_n t} \sin\omega_d t \tag{10}$$

where $\omega_d = \sqrt{1 - \zeta^2}\omega_n$. Since ζ is small, $\omega_d \approx \omega_n$. Equation (10) shows that the motor-side response contains a damped oscillation and a ramp component, and that increasing J_M or decreasing J_L can reduce oscillatory amplitudes, but a larger J_M or J_L results in a longer settling times.

For a two-mass system, the torsional torque (T_m) is

$$T_m = \int_0^{\theta_D} K d\theta = K\theta_D \tag{11}$$

where K is the torsional stiffness, and $\theta_D = \theta_M - \theta_L$. However, for MDTs, the coupling torque (T_C) is given by:

$$T_C = T_G \sin(p\theta_D) = \int_0^{\theta_D} T_G p \cos(p\theta) d\theta \tag{12}$$

Comparing (11) and (12), K_{lin} in (5) can be regarded as the torsional stiffness of MDTs under all operating conditions.

C. Problems induced by classical linearization conditions

In previous study [5], PI parameters for the control of MDTs are optimized through the ITAE criteria. Specifically, optimal coefficients of the fourth-order characteristic equation for step commands are given by

$$s^4 + 2.1\omega_c s^3 + 3.4\omega_c^2 s^2 + 2.7\omega_c^3 s + \omega_c^4 \tag{13}$$

where ω_c represents the -3 dB bandwidth. Consequently, the resulting PI parameters are

$$K_p \approx 1.85\omega_a J_L, \quad K_i \approx 0.6\omega_a^2 J_L \tag{14}$$

where ω_a is the anti-resonant frequency given by:

$$\omega_a = \sqrt{\frac{K}{J_L}} \tag{15}$$

Also, [5], [11], [12], regard K as being given by:

$$K = T_G p \tag{16}$$

which assumes linearisation of the dynamic model of the MDT under no-load conditions. Moreover, equations (5), (14), (15) and (16) show that the selection of controller parameters are dependant on ω_a, which itself is dependant on the linearized operating point. To make this point clearer, Fig. 2 shows the variation of ω_a as a function of the linearized operating point. It can be seen that linearizing around 60% to 80% of the pull-out torque can widen the performance envelope by referring back to (14).

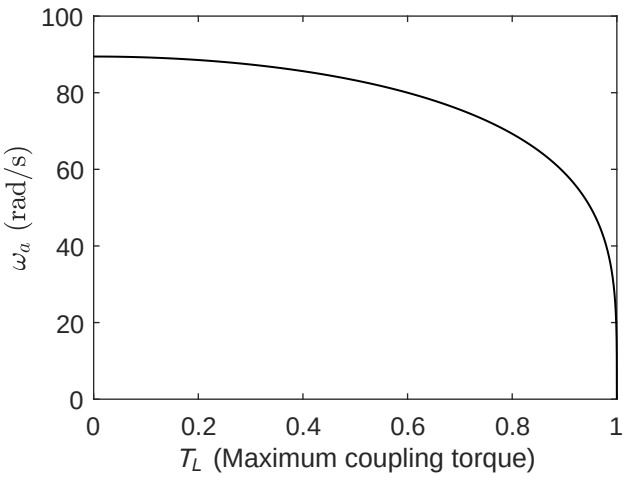

Fig. 2: ω_a versus T_L.

III. Speed Controller Design

A. Structure of 2DOF controller

2DOF controllers are well established methods of independently accommodating the design of reference tracking and disturbance rejection. Considering $F_c(s)$ shown in Fig.3 as a common PI controller $F_c(s) = K_p + K_i/s$, where K_p and K_i represent the proportional and integral coefficients. It can be seen that the 2DOF PI controller is a variant of more traditional PI schemes: a feed-forward controller $(F_{ff}(s))$ is adopted to enhance reference tracking, and a pre-filter $(F_{pf}(s))$ is employed to reduce or eliminate overshoot. For MDTs, the design of $F_{pf}(s)$ should specifically consider the system damping characteristics.

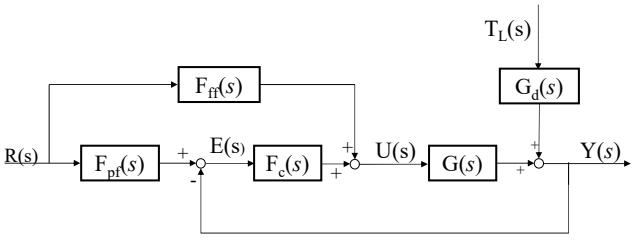

Fig. 3: Block diagram of the 2DOF PI control system.

To provide a concrete example of applying the methodologies to follow, we will focus on a typical practical system configuration. Linearizing the dynamics of the MDT test facility at 75% of the maximum coupling torque yields

$$G^{\omega_M}_{T_{em}}(s)|_{75\%} = \frac{1000\left(s^2+3s+5291\right)}{(s+3)\left(s^2+3s+10582\right)} \tag{17}$$

$$G^{\omega_M}_{T_L}(s)|_{75\%} = \frac{-5291000}{(s+3)\left(s^2+3s+10582\right)} \tag{18}$$

For simplicity, normalizing the angular velocity at $\omega_N = 125.7$ rad/s (1200 rpm) and the load-torque and electromagnetic torque at $T_G = 1.6\,\text{N·m}$, the normalized transfer functions are then:

$$N^{\omega_M}_{T_{em}}(s)|_{75\%} = \frac{12.7(5s^2+15s+26456)}{(s+3)(5s^2+15s+52912)} \tag{19}$$

$$N^{\omega_M}_{T_L}(s)|_{75\%} = \frac{-336750}{(s+3)(5s^2+15s+52912)} \tag{20}$$

Here, the plant and disturbance models are considered to be $G(s) = N^{\omega_M}_{T_{em}}(s)|_{75\%}$ and $G_d(s) = N^{\omega_M}_{T_L}(s)|_{75\%}$.

B. Design of pre-filter

Reference input shaping methods [22], [23] that exploit the spring dynamics of the controlled system to shape the reference command can greatly attenuate torsional oscillations, particularly for flexible and nonlinear systems. For 2DOF controllers that employ low-pass filters to shape step command inputs, the damped period is crucial for setting the time constant of the filter. Large time constants deteriorate command tracking performance whilst small time constants can induce speed oscillations. According to the robust shaper given in [23], desired incremental amplitudes (A_i) and time locations of impulses (t_i) are given by:

$$\begin{bmatrix} A_i \\ t_i \end{bmatrix} = \begin{bmatrix} \frac{1}{1+2\delta+\delta^2} & \frac{2\delta}{1+2\delta+\delta^2} & \frac{\delta^2}{1+2\delta+\delta^2} \\ 0 & 0.5T_d & T_d \end{bmatrix} \tag{21}$$

where $\delta = e^{-\frac{\zeta\pi}{\sqrt{1-\zeta^2}}}$, and T_d is the damped period of vibration. Equation (21) shows that at least a damped period is required to suppress oscillations in reference tracking. According to the definition of ω_n, the damped period of the MDT is given by

$$T_d = \sqrt{\frac{1}{K}\frac{J_M}{1+J_M/J_L}} \tag{22}$$

For the specific test facility considered here, $\delta \approx 1$. If a first order low-pass pre-filter is considered, $F_{pf}(s) = 1/(\tau_1 s+1)$, where τ_1 is the time constant, then the output of $F_{pf}(s)$ in response to a step input is given by:

$$F_{pf}(t) = 1 - e^{-t/\tau_1} \tag{23}$$

Now, $F_{pf}(t) \approx 0.25$, 0.75, and 0.95 at times $t = 0.28\tau_1$, $1.38\tau_1$, and $3\tau_1$, respectively. Thus, τ_1 can be set to $0.33T_d$. Supposing the MDT rig is allowed to run at 96% of the pull-out torque (that is $K|_{96\%}$ =$0.148K$, where $K|_{96\%}$ denotes the stiffness of the MDT running at 96% of the pull-out torque) and the actual load-side inertia J_L can be up to $2\hat{J}_L$ (where $\hat{J}_L$ is the estimated load-side inertia), taking the variation of the denominator of (22) into consideration, an acceptable time constant for the low-pass filter is $\tau_1 \approx T_d$.

Hence, the resulting pre-filter is given by:

$$F_{pf}(s) = \frac{1}{1+T_d s} \tag{24}$$

C. Design of feed-forward controller

As shown in Fig. 3, the transfer function from the reference R(s) to the output Y(s) is

$$T_{RY}(s) = \frac{\left(F_{pf}(s)F_c(s) + F_{ff}(s)\right)G(s)}{1 + F_c(s)G(s)} \tag{25}$$

To eliminate overshoot, we can choose ideal first order reference dynamics for the system, eg. $T_{RY}(s) = 1/(1+T_d s)$. From (25), the feed-forward loop is then immediately given by

$$F_{ff}(s) = \frac{1}{(1+T_d s)G(s)} \tag{26}$$

However, the anti-resonant frequency of the MDT decreases as load-torque increases. Hence, the zero, which contributes to the anti-resonant frequency, cannot be cancelled with (26). This means that first order dynamics can not be achieved with the transfer function $G(s)$ normalized at 75% of the pull-out torque. For simplicity, $F_{ff}(s)$ is approximated to $2(s+3)/\left(12.7(1+T_d s)\right)$ (referring to (19), if the bandwidth of closed-loop system is smaller than 23 rad/s, $5s^2$ and $15s$ are negligible while comparing to 26456 and 52912).

D. H_∞ mixed-sensitivity method of optimizing PI parameters

Field engineers can refer to [20] for a simple parameter setting method. But this strategy does not specify the bandwidth of load-torque disturbance and speed reference that the controller can accommodate. Here then, an alternative method is given based on H_∞ optimization to address these deficiencies.

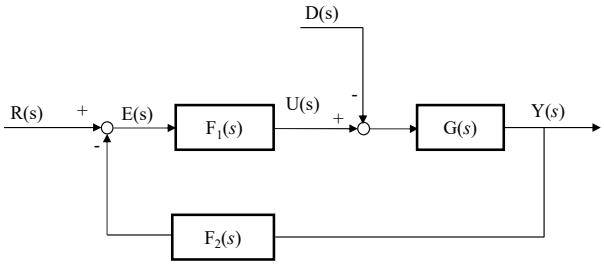

Fig. 4: Equivalent diagram of the 2DOF PI control system

Fig. 4 shows an equivalent diagram of the 2DOF PI control system (Fig. 3), where $D(s) = G_d(s)T_L(s)/G(s)$, $F_1(s)$ and $F_2(s)$ are given by

$$F_1(s) = F_{pf}(s)F_c(s) + F_{ff}(s) \tag{27}$$

$$F_2(s) = \frac{F_c(s)}{F_1(s)} \tag{28}$$

According to the equivalent structure, the error $E(s)$ and the control effort $U(s)$ are given by

$$E(s) = \frac{1}{1+G(s)F_c(s)}R(s) + \frac{F_2(s)G_d(s)}{1+G(s)F_c(s)}T_L(s) \tag{29}$$

$$U(s) = \frac{F_1(s)}{1+G(s)F_c(s)}R(s) + \frac{F_c(s)G_d(s)}{1+G(s)F_c(s)}T_L(s) \tag{30}$$

Defining $S_{de} = -\frac{F_2(s)G_d(s)}{1+G(s)F_c(s)}$, $S_{re} = \frac{1}{1+G(s)F_c(s)}$, $S_{du} = \frac{F_c(s)G_d(s)}{1+G(s)F_c(s)}$ and $S_{ru} = \frac{F_1(s)}{1+G(s)F_c(s)}$, (29) and (30) can be rewritten as

$$\begin{bmatrix} E(s) \\ U(s) \end{bmatrix} = \begin{bmatrix} S_{de} & S_{re} \\ S_{du} & S_{ru} \end{bmatrix} \begin{bmatrix} T_L(s) \\ R(s) \end{bmatrix} \tag{31}$$

Letting W_1 and W_2 be weighting filter functions, and

$$\|T(s)\|_\infty = \left\| \begin{bmatrix} W_1 S_{de} & W_1 S_{re} \\ W_2 S_{du} & W_2 S_{ru} \end{bmatrix} \right\|_\infty \tag{32}$$

the H_∞ mixed-sensitivity method is employed to obtain an optimized controller $F_c(s)$ which ensures $\|T(s)\|_\infty < 1$. For good reference-tracking and disturbance-rejection performance, W_1 is chosen to be relatively high inside the control bandwidth to obtain small S_{de} and S_{re}. For limiting the control effort to avoid initiating pole-slip requires selecting the sensitivity peak to obtain appropriate S_{du} and S_{ru}. Additionally, the bandwidth of W_2 should be set to be lower than the antiresonant frequency of the MDT.

Typically, weighting functions W_1 and W_2 are chosen to be of the form

$$W_1 = \frac{s/M + \omega_1}{s + A_1\omega_1} \tag{33}$$

$$W_2 = \frac{s + \omega_2/M}{A_2 s + \omega_2} \tag{34}$$

where A_1 and A_2 are the maximum allowed steady error, M is associated with the sensitivity peak, and ω_1 and ω_2 can be used to adjust the bandwidth of W_1 and W_2. Classically, M provides a means for assessing robustness. $M < 2$ indicates good robustness attributes, whilst $M > 4$ generally means both robustness and tracking performance will be poor. Hence, A_1, A_2 and M are the most readily determined parameters based on required specifications. In this case we choose $A_1 = A_2 = 0.05$, $M = 2$.

It can be seen from Fig. 2 that $\omega_a = 33.5$ rad/s while the MDT is operating at 99% of the pull-out torque. This means that the bandwidth ω_c of the speed control system should be set to a value less than 33.5 rad/s if a wide operational range is required. Here then we choose $\omega_1 = \omega_2 = 40$ rad/s (note: some iteration may be required in practice). Equation (32) and Fig. 5 shows that the steady-state error of speed regulation system increases when the frequencies of references and disturbances are greater than 2 rad/s, and that the gain of the controller significantly decreases when the frequencies are higher than 10 rad/s. Of note is that the maximum speed-loop bandwidth provided by the selected drives is 255 Hz; hence, the influence of the current control loop can be neglected in this design.

Using MATLAB's Robust Control Toolbox function $slTuner$ and $hinfstruct$ to calculate $\|T(s)\|_\infty$, the resulting parameters for the PI controller are:

$$K_p = 2.94, \quad K_i = 34.5 \tag{35}$$

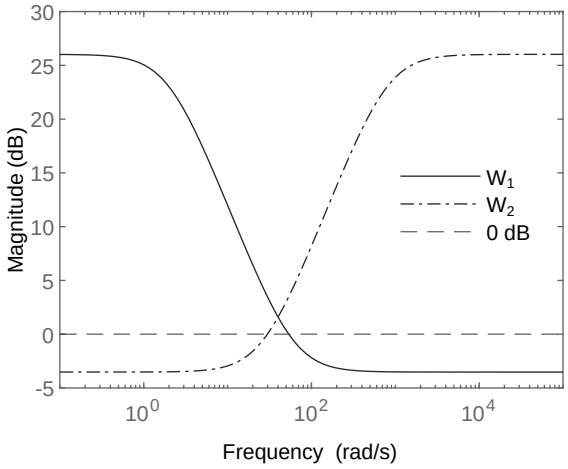

Fig. 5: Bode diagrams of weighting functions.

E. Robustness and stability analysis

To gain in terms of performance with respect to standard approaches, the phase margin (ϕ_m) of the speed control loop is adopted as a candidate performance metric. Fig. 6 shows that ϕ_m is approximately 70^0, albeit with some slight ϕ_m decrease as operating load-torque increases. For classic design methods proposed for speed control of electrical drives, this value is considered sufficient to provide robust performance (see [17]). However, MDT control systems cannot simply be analysed using classic methods. MDTs can enter a pole-slipping regime induced by speed reference changes or load-torque distur-b

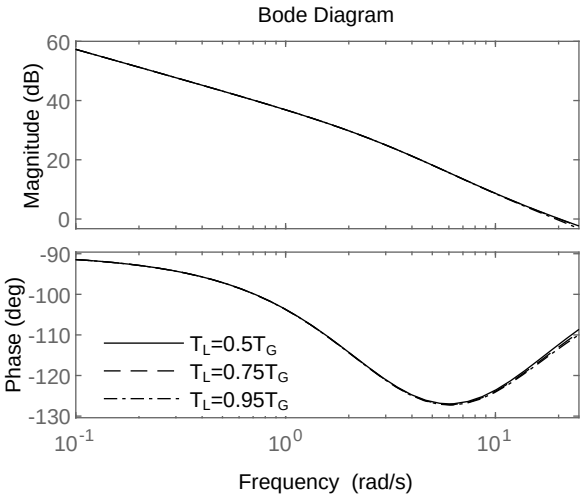

Fig. 6: Open loop responses of the speed control system under 50%, 75% and 95% of the pull-out torque.

Letting T_{fl} and T_{fm} denote the load- and motor-side friction torque, when the MDT is operating normally, the coupling torque (T_C) and developed motor torque (T_{em}) are described by

$$T_C = T_L + T_{fl} \tag{36}$$

$$T_{em} = T_C + T_{fm} \tag{37}$$

From (36) and (37), it can be seen that either $T_L + T_{fl} > T_G$ or $T_{em} > T_G + T_{fm}$ invokes pole-slipping.

The peak value of T_{em} is determined by S_{ru} and S_{du}. Examination of S_{ru} and S_{du}, shows that if:

$$\omega_{c2} > \omega_c > \omega_{c1} \tag{38}$$

where $\omega_{c1} = \frac{3(B_M+B_L)}{J_M+J_L}$ and $\omega_{c2} = \frac{1}{3}\min\left(\sqrt{\frac{(J_M+J_L)K_{\text{lin}}}{J_M J_L}}, \sqrt{\frac{(B_M+B_L)K_{\text{lin}}}{J_M B_L + B_M J_L}}, \sqrt{\frac{K_{\text{lin}}}{J_L}}, \frac{K_{\text{lin}}}{B_L}\right)$, then S_{ru} can be simplified to

$$S_{ru} \approx \frac{\omega_N (J_M + J_L)\, s}{T_G (T_d s + 1)} \tag{39}$$

, and S_{du} is described by

$$S_{du} \approx \frac{T_G K_{\text{lin}} (K_p s + K_i)}{J_M J_L \omega_N s^4 + (J_M + J_L)\omega_N s^2 + (K_p s + K_i) T_G K_{\text{lin}}} \tag{40}$$

Inversing Laplace transforming (39) yields

$$S_{ru}(t) = \frac{\omega_N (J_M + J_L)}{T_G T_d}\delta(t) - \frac{\omega_N (J_M + J_L)}{T_G T_d^2} e^{-\frac{t}{T_d}} \tag{41}$$

Equations (39) and (41) show that the sensitivity peak of S_{ru} will significantly increase as J_L increases. However, as shown in (41) and Fig. 7, this problem can be addressed by adjusting the settings of speed reference (r) or time constant (T_d). Moreover, (40) indicates that increases in J_L results a large peak in S_{du}. It can be seen from Fig. 8 that while the inertia ratio (IR) rises from 1 to 5, the sensitivity peak of S_{du} increases accordingly from 1.2 to 1.4. It means the maximum permitted load-torque disturbance reduces from $0.83T_G$ to $0.71T_G$ (assuming friction torque is negligible in this case).

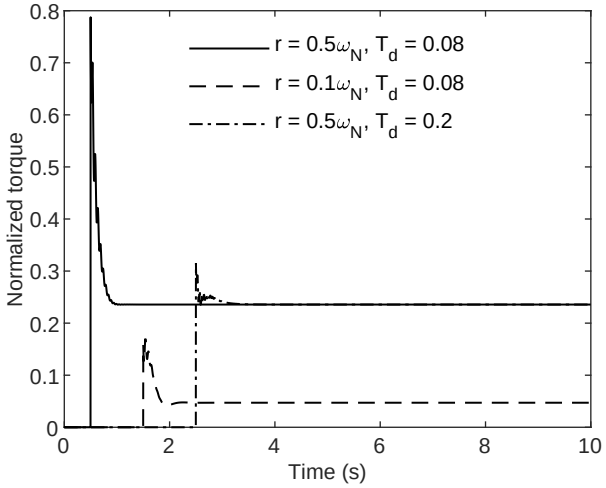

Fig. 7: Simulated control effort of experimental test facility with various parameter settings (speed references are imposed at 0.5 s, 1.5 s and 2.5 s, respectively).

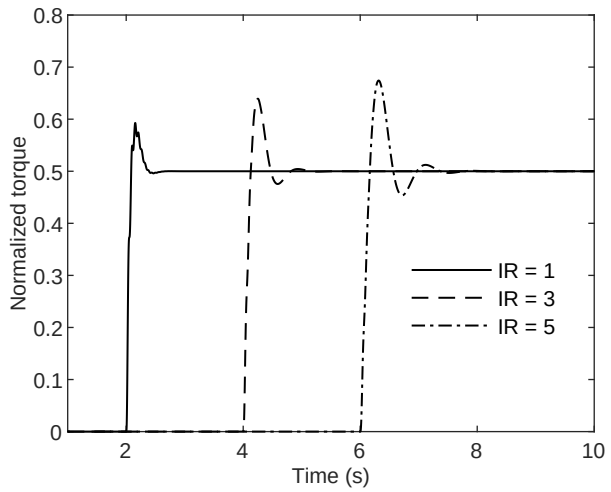

Fig. 8: Simulated control effort with regard to load-torque disturbances ($T_L = 0.5T_G$, load-torque disturbances are imposed at 0.5 s, 1.5 s and 2.5 s, respectively).

Let U_{s1} and U_{s2} denote the steady-state values (time-domain) of S_{ru} and S_{du}, respectively. Then U_{s1} and U_{s2} are, respectively, given by

$$\begin{aligned} U_{s1} &= T_{fm} + T_{fl} \\ U_{s2} &= T_L \end{aligned} \tag{42}$$

Equation (41) shows that the peak value of Fig. 7 is impulsive, and can be partly damped by the delays related to current control loops. Hence, according to Fig. 7 and Fig. 8, the maximum controller output caused by the speed reference r and load-torque disturbance T_L are, respectively, described by

$$U_{rm} \approx 0.95r, \quad U_{dm} \approx 1.2T_L \tag{43}$$

Criteria for MDTs to maintain a normal running with respect to speed references or load-torque disturbances are therefore given by

$$U_{s1} + U_{s2} + U_{dm} < T_G + T_{fm} \tag{44}$$

$$U_{s1} + U_{s2} + U_{rm} < T_G + T_{fm} \tag{45}$$

Two example scenarios based on the previous analysis are now considered.

Example 1: Assume the MDT rig is initially operating at $0.67\omega_N$ (800 rpm) under no-load torque, find the maximum permitted load-torque disturbance (T_{md}) that will not initiate pole-slipping.

The friction torque with respect to motor- and load-side components are $T_{fm} = B_M\omega_M = 0.16T_G$ and $T_{fl} = T_{fm}$, respectively. According to (42), $U_{s1} = 0.32T_G$, and no-load torque gives $U_{s2} = 0$. Therefore, the maximum increment of control effort given by (44) is $U_{dm} = T_G - 0.16T_G = 0.84T_G$, and the resulting T_{md} from (43) is $0.84T_G/1.2 = 0.7T_G$.

Example 2: When the MDT rig is running at $0.33\omega_N$ (400 rpm) under 70% of the pull-out torque, find the maximum speed command increment (r_m) that will not initiate pole-slipping.

The motor- and load-side friction torque corresponding to $0.33\omega_N$ are $T_{fm} = T_{fl} = 0.08T_G$. According to (42), U_{s1} is therefore $0.16T_G$. Moreover, $T_L = 0.7T_G$ gives $U_{s2} = 0.7T_G$. Assuming the friction torque developed by the speed increment is negligible, then the maximum increase of control effort given by (45) is $U_{rm} = (1 - 0.7 - 0.08)T_G = 0.22T_G$. Hence, the resulting r_m from (43) is $0.22\omega_N/0.95 = 0.23\omega_N$ (=278 rpm).

IV. Position Controller Design

Having addressed speed control dynamics, we now turn attention to position tracking. In [21], a PDF controller was employed to achieve servo control of an MDT encompassing magnetic gears, and the position reference is given directly as a step input signal. However, MDTs have a maximum permitted speed (V_p) that is determined by the maximum permitted load-torque disturbance and friction torque, to prevent pole-slipping. Hence, a simple PDF position controller may generate an aggressive speed demand as a result of large position change demands; consequently, speed oscillations or even pole-slipping can be induced.

A. Position references

Suppose the MDT is required to take a maximum of $3T_d$ to reach V_p, and a further $3T_d$ to decelerate from V_p to 0. Thus, the optimal solution for position regulation is the MDT running at V_p except during acceleration/deceleration periods. Fig. 9 therefore provides a desirable speed reference to achieve position regulation.

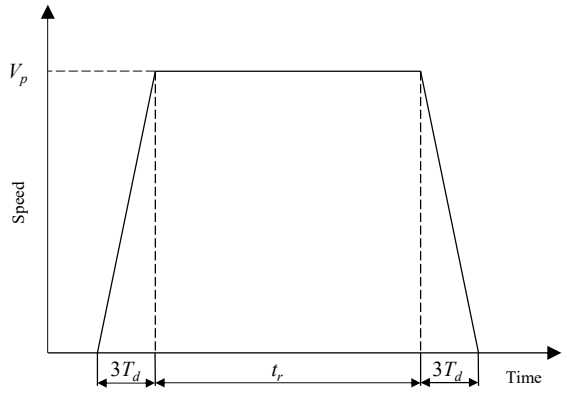

Fig. 9: Desired speed reference

Consider P_{os} to be the reference position, when $P_{os} \leq 3V_pT_d$ the driving motor can be scheduled to advance in incremental steps smaller than $\pi/2p$ over fixed (constant) time intervals, which is the maximum increment that does not initiate pole-slipping. A solution therefore readily exists for this condition. Therefore, we now consider conditions where $P_{os} > 3V_pT_d$. Letting t_r represents the running time under V_p, then, t_r is given by

$$t_r = (P_{os} - 3V_pT_d)/V_p \tag{46}$$

and the acceleration/deceleration rate is $a = V_p/3T_d$. Hence, the position reference signal R_p with the desired reference speed profile is scheduled as:

$$R_p = \begin{cases} s_1 & t \le 3T_d \\ s_2 & 3T_d < t \le 3T_d + t_r \\ s_3 & t_r + 3T_d < t \le t_r + 6T_d \\ P_{os} & t > t_r + 6T_d \end{cases} \tag{47}$$

where $s_1 = \frac{1}{2}at^2$, $s_2 = \frac{9}{2}aT_d^2 + V_p\,(t - 3T_d)$, $s_3 = -\frac{1}{2}at^2 + V_pt - \frac{1}{2}a\,(t - t_r - 3T_d)$.

B. Design of position controller

As load-torque disturbances have been rejected by the 2DOF PI speed controller, the position controller can then be designed as a simple proportional controller. The position reference for this application is defined by (47), which cannot be considered as either a classical step or ramp. Here then, we employ another optimization method rather than calculating parameters directly from the characteristic equations in (13). From Fig. 4, the speed control loop dynamics are given by

$$G_s(s) = \frac{F_1(s)G(s)}{1 + F_1(s)F_2(s)G(s)} \tag{48}$$

Fig. 10 illustrates the principle of optimizing the parameter for the position controller through a servo control block diagram.

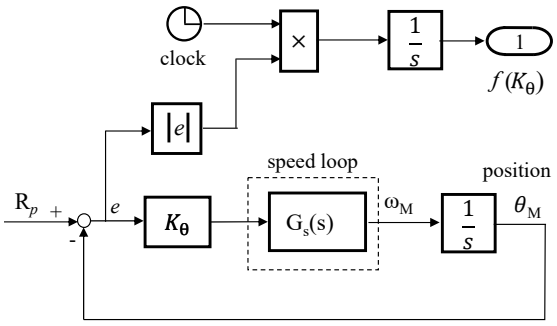

Fig. 10: Block diagram to obtain an optimized K_θ.

The ITAE performance index can be regarded as a function of K_θ, that is

$$\text{ITAE} = \int_0^T t|e(t)|dt = f(K_\theta) \tag{49}$$

where T is the running time. Then, the problem of finding an optimized K_θ can be converted into a problem to search for $\min_{K_\theta} f(K_\theta)$. Here, the $fminsearch$ function provided by the Matlab optimization toolbox is employed to find a solution, and the optimized result is

$$K_\theta = 1.50 \tag{50}$$

V. Simulation and Experimental Results

To show the implementation and performance of the proposed control strategies during extreme operating conditions, we will again consider the scenario specified in Example 1. Taking the resolution of output electromagnetic torque into consideration, the load-torque disturbance is set to $0.67T_G$ rather than $0.7T_G$. Because the position encoder integrated with the servo motor only offers 12-bit resolution, the period of speed control loop is set to 4 ms to ensure the accuracy of speed measurement. The algorithm is discretized with the zero-order hold method due to control inputs are supposed to be piecewise constant over the sample time.

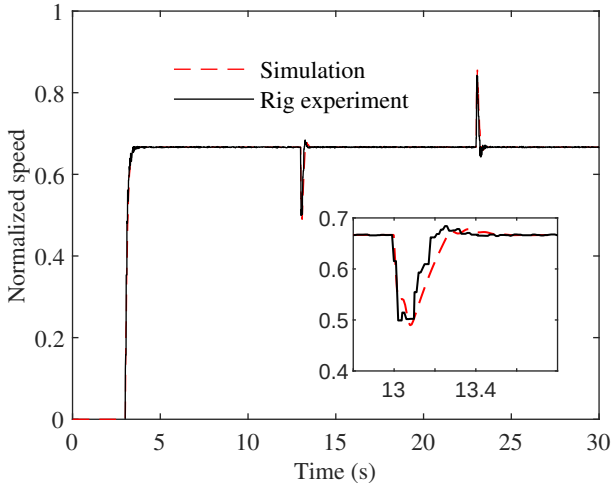

Fig. 11: Simulated and experimental results of the motor-side shaft with $\tau_1 = T_d$, $K_p = 2.9, K_i = 34.5$ ($r = 0.67\omega_N$, $T_L = 0\,\text{N·m}$, $0.67T_G$ and $0\,\text{N·m}$ at 3-13 s, 13-23 s and 23-30 s, respectively).

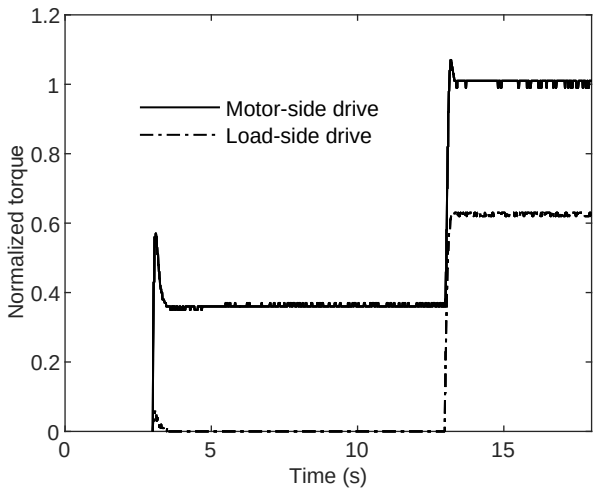

Fig. 12: The electromagnetic torque outputs of two drives.

Fig. 11 shows the motor-side speed of simulation is seen to match the experimental test facility measurements over a wide

operating range. Fig. 12 plots the output of electromagnetic torque of two drives and validates the sensitivity peak analysis described by (40), (41), (43), Fig. 7 and Fig. 8. It can be seen from Fig. 12 that whilst the load-torque is greater than $0.7T_G$, T_{em} will breach the stable running criterion given by (44) (T_{em} is normalized at the maximum coupling torque T_G).

Referring to the experimental results of Fig. 13 where the time constant (τ_1) of the pre-filter is set to $0.6T_d$ (the recommended τ_1 is T_d), the load-side coupling enters a pole-slipping operating regime when the speed command $0.67\omega_N$ is given at 3 s.

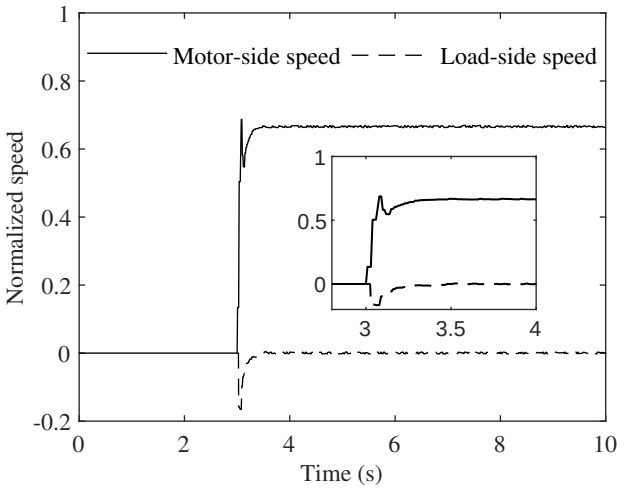

Fig. 13: Experimental measurements of pole-slipping with $\tau_1 = 0.6T_d$, $K_p = 2.9, K_i = 34.5$ and $T_L = 0\,\text{N·m}$.

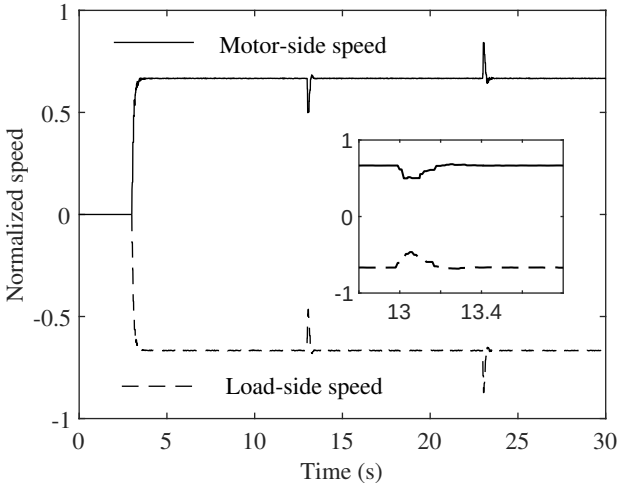

Fig. 14: Experimental measurements of speed at both side of the coupling with $\tau_1 = T_d$, $K_p = 2.9, K_i = 34.5$ ($T_L = 0\,\text{N·m}$, $0.67T_G$ and $0\,\text{N·m}$ at 3-13 s, 13-23 s and 23-30 s, respectively).

Fig. 14 represents very good load-side vs. motor-side coupling using the proposed pre-filter design even when subject to extreme load disturbances. The results presented in Fig. 11, Fig. 13 and Fig. 14 indicate that designing 2DOF PI controllers with the spring characteristic parameters (T_d and ω_a) and model linearized at 75% of the pull-out torque prevents the MDT from induced speed oscillations and pole-slipping resulting from aggressive speed commands and load-torque disturbances. Further, these results are achieved without direct measurement of load-side speed.

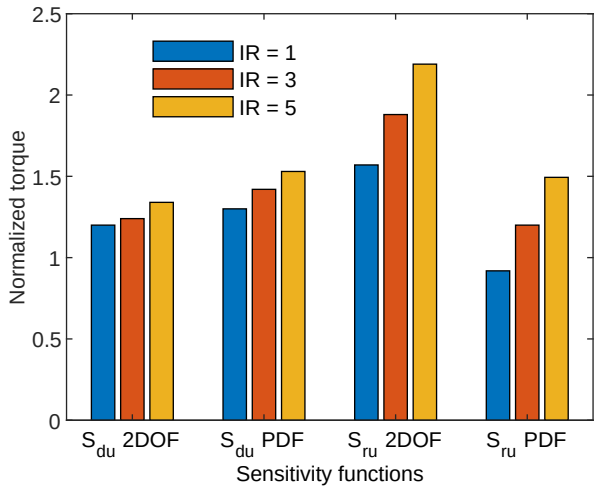

Fig. 15: The sensitivity peaks of S_{ru} and S_{du} (r and d are modelled as step inputs, the delays associated with current control loops are not taken into consideration).

Fig. 15 shows the maximum controller outputs generated by speed references and load-torque disturbances with regard to the optimized 2DOF PI controller and the benchmark PDF controller proposed by [1]. It can be seen from Fig. 15 that 1) the proposed design can accommodate a wider range of load-torque disturbance and is more robust to load-side inertia variations, and 2) the optimized 2DOF controller offers a faster speed response (piecewise speed references are recommended here).

It can be seen from Fig. 16 that the proposed strategy provides the required acceleration/deceleration responses for position regulation. Moreover, Fig. 16 shows that the 2DOF PI controller substantially rejects the extreme load-torque disturbance that that is applied between 0 N·m and 67% of the pull-out torque and then restores the no-load condition, and that the proportional controller achieves zero steady-state error position tracking without the feedback of load-side position measurements.

VI. Conclusion

Through discussions of models of MDTs with nonlinear stiffness characteristics, appropriate linearization, 2DOF PI speed regulation system design, and position control strategies, the paper has addressed the most important issues of servo control of drive-trains incorporating magnetic couplings. Speed regulation measurements show outstanding performance in reference tracking and load-torque disturbance rejection.

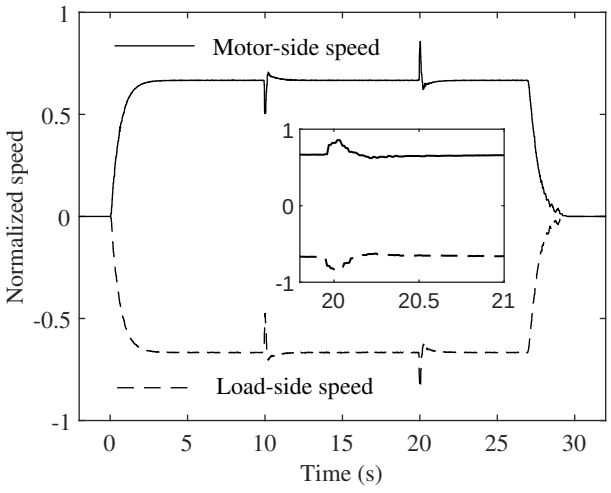

(a)

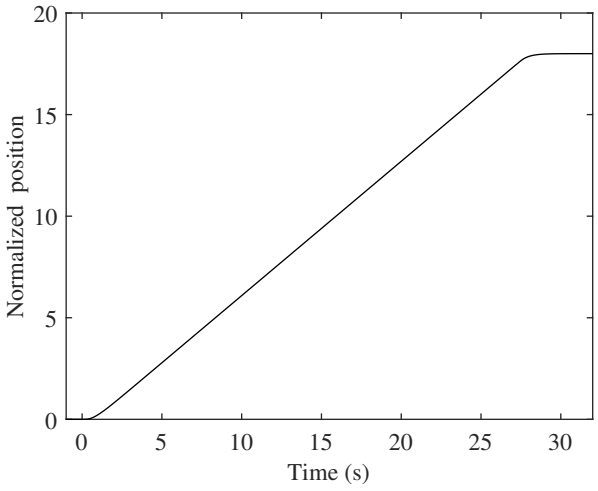

(b)

Fig. 16: Experimental measurements (a) operating speed (b) load-side position ($R_p = 18$, $T_L = 0\,\mathrm{N{\cdot}m}$, $0.67T_G$ and $0\,\mathrm{N{\cdot}m}$ at 0-10 s, 10-20 s and 20-35 s, respectively).

Moreover, experimental results reveal that the developed position control strategy achieves no over-shoot in position tracking without the need for load-side measurements. Although the speed and position controller design methodologies presented here have specifically focused on the control of MDTs with nonlinear stiffness characteristics, the underlying principles are also more generally applicable to other more traditional dual-mass drive systems.

REFERENCES

[1] X. Zhu, Z. Xiang, L. Quan, Y. Chen, and L. Mo, "Multimode optimization research on a multiport magnetic planetary gear permanent magnet machine for hybrid electric vehicles," *IEEE Transactions on Industrial Electronics*, vol. 65, no. 11, pp. 9035–9046, 2018.

[2] M. Benarous and M. Trezieres, "Design of a cost-effective magnetic gearbox for an aerospace application," *The Journal of Engineering*, vol. 2019, no. 17, pp. 4081–4084, 2019.

[3] B. McGilton, R. Crozier, A. McDonald, and M. Mueller, "Review of magnetic gear technologies and their applications in marine energy," *IET Renewable Power Generation*, vol. 12, no. 2, pp. 174–181, 2017.

[4] M. Desvaux, R. L. G. Latimier, B. Multon, H. B. Ahmed, and S. Sire, "Design and optimization of magnetic gears with arrangement and mechanical constraints for wind turbine applications," in *2016 Eleventh International Conference on Ecological Vehicles and Renewable Energies (EVER)*. IEEE, 2016, pp. 1–8.

[5] R. Montague, C. Bingham, and K. Atallah, "Servo control of magnetic gears," *IEEE/ASME Transactions on Mechatronics*, vol. 17, no. 2, pp. 269–278, 2011.

[6] R. Montague and C. Bingham, "Nonlinear control of magnetically-geared drive-trains," *International Journal of Automation and Computing*, vol. 10, no. 4, pp. 319–326, 2013.

[7] D. Y. Ohm, "Analysis of pid and pdf compensators for motion control systems," in *Proceedings of 1994 IEEE Industry Applications Society Annual Meeting*, vol. 2. IEEE, 1994, pp. 1923–1929.

[8] S. Cheng, Y.-Y. Huang, and H.-H. Chou, "Dual robust controller design for high power ac servo drive," in *2008 ECSIS Symposium on Learning and Adaptive Behaviors for Robotic Systems (LAB-RS)*. IEEE, 2008, pp. 97–102.

[9] S. E. Saarakkala and M. Hinkkanen, "State-space speed control of two-mass mechanical systems: Analytical tuning and experimental evaluation," *IEEE Transactions on Industry Applications*, vol. 50, no. 5, pp. 3428–3437, 2014.

[10] S. Morimoto, A. Hamamoto, and Y. Takeda, "Vibration control of two-mass system with low inertia ratio considering practical use," *Electrical engineering in japan*, vol. 125, no. 2, pp. 1–9, 1998.

[11] C. Di Natali, J. Buzzi, N. Garbin, M. Beccani, and P. Valdastri, "Closed-loop control of local magnetic actuation for robotic surgical instruments," *IEEE Transactions on Robotics*, vol. 31, no. 1, pp. 143–156, 2015.

[12] R. G. Montague, C. Bingham, and K. Atallah, "Magnetic gear pole-slip prevention using explicit model predictive control," *IEEE/ASME Transactions on Mechatronics*, vol. 18, no. 5, pp. 1535–1543, 2012.

[13] M. Bouheraoua, J. Wang, and K. Atallah, "Design and implementation of an observer-based state feedback controller for a pseudo direct drive," *IET Electric Power Applications*, vol. 7, no. 8, pp. 643–653, 2013.

[14] M. Bouheraoua, J. Wang, and K. Atallah, "Slip recovery and prevention in pseudo direct drive permanent-magnet machines," *IEEE transactions on industry applications*, vol. 51, no. 3, pp. 2291–2299, 2014.

[15] M. Bouheraoua, J. Wang, and K. Atallah, "Speed control for a pseudo direct drive permanent-magnet machine with one position sensor on low-speed rotor," *IEEE transactions on industry applications*, vol. 50, no. 6, pp. 3825–3833, 2014.

[16] Y. Hori, H. Sawada, and Y. Chun, "Slow resonance ratio control for vibration suppression and disturbance rejection in torsional system," *IEEE Transactions on Industrial Electronics*, vol. 46, no. 1, pp. 162–168, 1999.

[17] L. Harnefors, S. E. Saarakkala, and M. Hinkkanen, "Speed control of electrical drives using classical control methods," *IEEE Transactions on Industry Applications*, vol. 49, no. 2, pp. 889–898, 2013.

[18] C. Xia, B. Ji, T. Shi, and Y. Yan, "Two-degree-of-freedom proportional integral speed control of electrical drives with kalman-filter-based speed estimation," *IET Electric Power Applications*, vol. 10, no. 1, pp. 18–24, 2016.

[19] F. Mendoza-Mondragón, V. M. Hernández-Guzmán, and J. Rodríguez-Reséndiz, "Robust speed control of permanent magnet synchronous motors using two-degrees-of-freedom control," *IEEE Transactions on Industrial Electronics*, vol. 65, no. 8, pp. 6099–6108, 2018.

[20] X. Liao, C. Bingham, A. Zolotas, Q. Zhang, and T. Smith, "Speed control of drive-train incorporating magnetic coupling," in *2020 International Conference on Electrical Machines (ICEM)*, vol. 1. IEEE, 2020, pp. 1225–1231.

[21] R. Montague, C. Bingham, and K. Atallah, "Dual-observer-based position-servo control of a magnetic gear," *IET electric power applications*, vol. 5, no. 9, pp. 708–714, 2011.

[22] W. Singhose, R. Eloundou, and J. Lawrence, "Command generation for flexible systems by input shaping and command smoothing," *Journal of guidance, control, and dynamics*, vol. 33, no. 6, pp. 1697–1707, 2010.

[23] S. Brock and M. Gniadek, "Robust input shaping for two-mass system with variable parameters," *Poznan University of Technology Academic Journals. Electrical Engineering*, no. 77, pp. 209–215, 2014.

2022-03-18

Servo control of drive-trains incorporating magnetic couplings

Liao, Xiaowen

IEEE

Liao X, Bingham C, Zolotas A, et al., (2022) Servo control of drive-trains incorporating magnetic couplings, IEEE Transactions on Industry Applications, Volume 58, Number 3, May-June 2022, pp. 3674-3684

https://doi.org/10.1109/TIA.2022.3160680